ISSN: 0067-2904

Influence of a Magnetic Field on the Structure, Morphology and Gas Sensing Characteristics of ZnO: Al Thin Films Prepared by Pulsed Laser Ablation

Zahraa Marid Abbas*, Qusay Adnan Abbas
Department of Physics, College of Science, University of Baghdad, Baghdad, Iraq

Received: 29/12/2022 Accepted: 19/4/2023 Published: 30/4/2024

Abstract

In this work, aluminium-doped zinc oxide (AZO) nanostructure at 0.3 wt% and 0.5 wt% Al was synthesized using the pulse-laser ablation technique in liquid(PLAL) using pulsed Nd: YAG laser of a fundamental wavelength of (1064 nm). The process was done in the absence and presence of an external magnetic field. The deposited AZO nanostructures by drop-casting on etched-Si wafers were examined by different techniques. The XRD test illustrates enhancing the crystallinity of the prepared thin films by applying an external magnetic field. The FESEM images displayed the change of nanostructure to nano-sheets of high surface area after using a 77.2 mT permanent magnet placed behind the target during the ablation process. The gas sensor based on the AZO nanostructures has higher sensitivity against NO_2 than H_2S. Increasing the Al ratio from 0.3 wt% to 0.5 wt% changed the properties of the prepared samples to have small porosity and small surface area, which negatively affected the properties of the sensor

Keywords: gas sensing, ZnO: Al nanostructures, pulse laser ablation, XRD, SEM.

تأثير المجال المغناطيسي على خصائص الطبوغرافية والتركيبية والتحسسية للغازات لأغشية أوكسيد الزنك:الالمنيوم المحضرة بطريقة الاستئصال بالليزر النبضي

زهراء مارد عباس*, قصي عدنان عباس
قسم الفيزياء ، كلية العلوم ، جامعة بغداد ، بغداد ، العراق

الخلاصة

تم في هذا العمل تصنيع الهياكل النانوية لأوكسيد الزنك المشوب بالألمنيوم (AZO) بنسبة ذرية 0.3 و0.5 من الألمنيوم باستخدام تقنية الاجتثاث بالليزر النبضي في السائل باستخدام ليزر Nd:YAG ذو الطول الموجي الأساسي (1064 نانومتر). تمت العملية في غياب ووجود مجال مغناطيسي خارجي. تم فحص الهياكل النانوية *AZO* المحضرة بطريقة الصب على رقائق السليكون المحفورة بالعديد من التقنيات. يوضح اختبار XRD تعزيز تبلور الأغشية الرقيقة المحضرة بتطبيق مجال مغناطيسي خارجي. عرضت صور SEM تباين البنية النانوية إلى صفائح نانوية ذات مساحة سطحية عالية بعد استخدام مغناطيس دائم 77.2 mT خلف الهدف أثناء عملية الاجتثاث. مستشعر الغاز المعتمد على الهياكل النانوية (AZO) لديه حساسية أعلى في NO2 من

*Email: zahraamarid92@gmail.com

H2S. تؤدي زيادة نسبة الألمنيوم من 0.3 الى 0.5 بتدهور خصائص العينات المحضرة لتصبح ذات مسامية صغيرة ومساحة سطحية صغيرة، مما أثر سلباً على خصائص المستشعر.

1. Introduction

Metal oxides are one of the most stable materials in nature; they have been used in many modern applications. Zinc oxide (ZnO) is one of these metal oxides, which has a wide bandgap; it is an n-type semiconductor which has been used in many applications [1], including solar cells [3], UV detectors [4], sensors [5], etc. It is non-toxic, has high stability, and high transmittance [2]. Pure and doped ZnO thin films have been fabricated by several techniques, including chemical bath deposition [6], sol-gel [7], pulsed laser deposition [8], etc.

The target properties highly affect the laser-induced nanostructures prepared by the PLD technique [11]. It was found experimentally that using an external magnetic field with the (PLD) technique improves the target ablation process and highly affects the formation of laser-induced nanostructures [10,12, 13]. It was reported that applying a tangential magnetic field increases the surface morphology and growth rate of the formed material [14].

ZnO thin film properties, such as the optical bandgap, change when the oxide is mixed with metals. ZnO: Al mixture is an alternative transparent conductive oxide layer [15]. Some studies showed the formation of doped ZnO with different nanostructures depended on the deposition technique, deposition parameters, and doping types such as nanorods [16], nanosheets [17], clusters [18], etc.

In this work, the effect of applying an external magnetic field during the ablation of ZnO:Al at 0.3 % and 0.5 wt% Al was studied. Also, the effect of operating temperature, Al content and magnetic field on the sensitivity of the AZO-based gas sensors was studied for NO_2 and H_2S gases.

1. Experimental part

Aluminum Zinc oxide(AZO) mixture of 0.3 and 0.5 wt% aluminum was formed into disc capsules of 1 cm in diameter and 0.5 cm thick by pressing their mixed powder using a stainless-steel mould under 5 tons press for 15 min. The AZO nanoparticles were prepared by pulsed laser ablation in liquid (PLAL)technique in 3 ml distilled water using Nd-YAG laser of 200 pulses of 9 nanoseconds pulse-duration at 6 Hz repetition rate and 400 mJ pulse energy. AZO nanoparticles were also prepared with a 77.2 mT permanent magnet placed behind the target. The AZO thin films were formed by depositing the AZO nanoparticles on 2×2 cm^2 glass substrates on a hot plate at 70 °C by drop-casting.

The structural properties of the samples were examined by X-Ray diffractometer (Philips X'PERT MPD - MRL UCSB), field emission-scanning electron microscope (Ultra-high Resolution FE-SEM SU9000), FTIR (Tensor-27, Bruker Optics Inc), and UV-Visible absorbance spectroscope (UV-Vis-NIR Metertech SP-8001).

Mesh electrodes of Al were deposited under a high vacuum using a compact thermal evaporation coating system (Edwards E306A) under high vacuum. Figure (1) shows schematically the steps of sample preparation and gas sensor fabrication. The gas sensors based on the prepared AZO samples were tested for NO_2 and H_2S gases on a controlled temperature substrate (which was controlled by a thermocouple and thermometer) in a closed chamber of 4000 cc volume with a removable cover fixed by an O–ring rubber. Subsequently, gas-air mixture and clean air flow through the chamber via electrical valves for specific periods of time. A multi-pin feed-through at the base of the chamber allows the electrical connections to

be established to the heater and the sensor electrodes. A PC –interfaced multimeter (type UNI-T UT81B) was used to monitor the resistance variation of the sample.

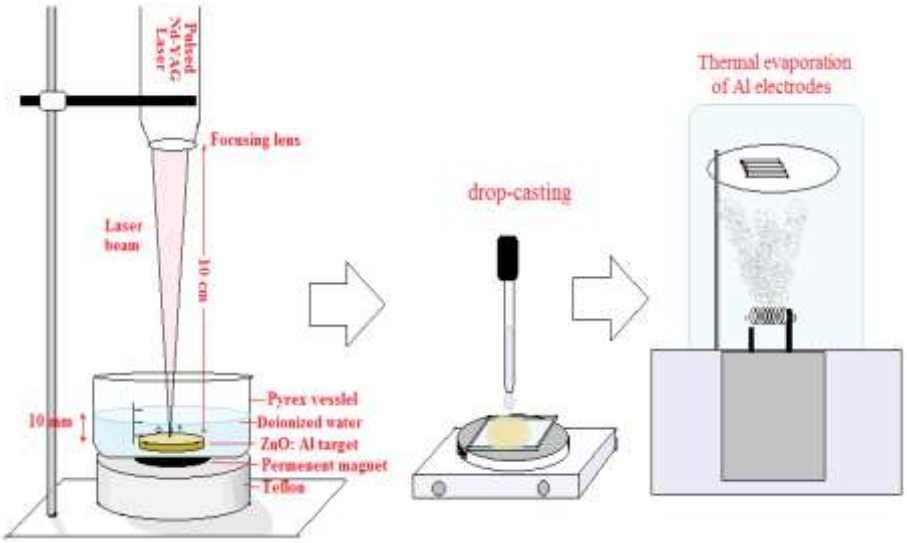

Figure 1: Schematic diagram of experimental sample preparation and gas sensor fabrication.

2. Results and Discussion

Figure (2) shows the X-ray diffraction patterns for the deposited AZO nanoparticles on the etched silicon, prepared without and with an external magnetic field. The diffraction patterns matched the standard lines for the hexagonal ZnO structure according to card No. (79-2205). The inter-planner distances (d_{hkl}) were determined using Bragg's law, and the crystalline size (D) was determined by Scherrer's formula. The results are listed in Table (1) [19]. The crystallinity enhanced, and the crystallite size increased after applying the magnetic field due to the plasma confinement effect, which caused an increase in plasma density and temperature. The created clusters inside the plasma may be heated by collisions with electrons. The collision frequency increased and acted more effectively as a heating source during the cluster growth. The delay in the cooling process caused an increase in the growth size with enhanced crystallinity [20, 21].

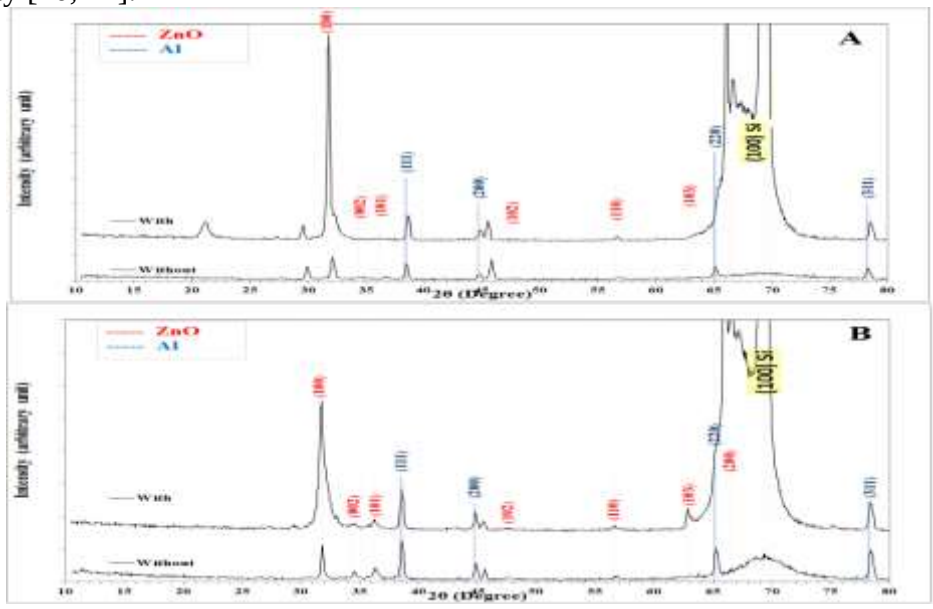

Figure 2: XRD patterns of AZO on P-Si prepared without and with the magnetic field at (A) 0.3 wt% and (B) 0.5 wt% Al.

The patterns showed peaks corresponding to the aluminium phase in the composite samples. The peaks corresponding to this phase increased in intensity with increasing the aluminium ratio from 0.3 to 0.5 wt%.

Table 1: XRD characteristics of AZO on P-Si without and with the magnetic field at 0.3 wt% and 0.5 wt% Al ratios.

Sample	Magnetic	2θ (Deg.)	FWHM (Deg.)	d_{hkl} Exp.(Å)	D (nm)	hkl	Phase
0.3 Al 400 mJ	Without	31.7599	0.4605	2.8152	17.9	(100)	Hex. ZnO
		38.6294	0.4605	2.3289	18.3	(111)	Cub. Al
		44.8465	0.3838	2.0194	22.4	(200)	Cub. Al
		78.4649	0.4989	1.2179	20.6	(311)	Cub. Al
	With	32.1820	0.3838	2.7792	21.6	(100)	Hex. ZnO
		34.4079	0.5756	2.6044	14.5	(002)	Hex. ZnO
		36.6721	0.6524	2.4486	12.8	(101)	Hex. ZnO
		38.5526	0.3838	2.3334	21.9	(111)	Cub. Al
		44.8849	0.4222	2.0178	20.4	(200)	Cub. Al
		78.3498	0.4989	1.2194	20.5	(311)	Cub. Al
0.5 Al 400 mJ	without	31.7366	0.3220	2.8172	25.7	(100)	Hex. ZnO
		34.4738	0.3623	2.5995	23.0	(002)	Hex. ZnO
		36.3657	0.5635	2.4685	14.8	(101)	Hex. ZnO
		38.5796	0.3623	2.3318	23.2	(111)	Cub. Al
		44.8591	0.3623	2.0189	23.7	(200)	Cub. Al
		78.4301	0.4428	1.2184	23.2	(311)	Cub. Al
	with	31.8171	1.0063	2.8103	8.2	(100)	Hex. ZnO
		34.3933	0.7246	2.6054	11.5	(002)	Hex. ZnO
		36.2852	0.6843	2.4738	12.2	(101)	Hex. ZnO
		38.5394	0.3623	2.3341	23.2	(111)	Cub. Al
		44.8189	0.3220	2.0206	26.7	(200)	Cub. Al
		78.3496	0.4831	1.2194	21.2	(311)	Cub. Al

The surface morphology of the prepared AZO NPs of 0.3 wt% and 0.5 wt% Al using the PLAL without and with a magnetic field is shown in Figure (3). The sample surface behaviour varies according to the Al ratio and the presence of the magnetic field. The ZnO: $Al_{0.3}$ without the magnetic field appeared as inhomogeneously distributed flakes merging among each other, constructing a high porosity surface. With the magnetic field, the construction was formed with larger number of folds. The formation of zinc as a bonded multilayer nano-sheets structure was shown in a previous study [22]. Increasing the Al ratio to 0.5 wt% caused the disappearance of the flake structures and the reduction of the sample porosity. So, the nanostructure of the sample surface and the size distribution of the AZO were greatly influenced by the different preparation conditions; so the variation in the surface area and the connecting mode between adjacent nanostructures may highly affect the gas sensitivity performances [23].

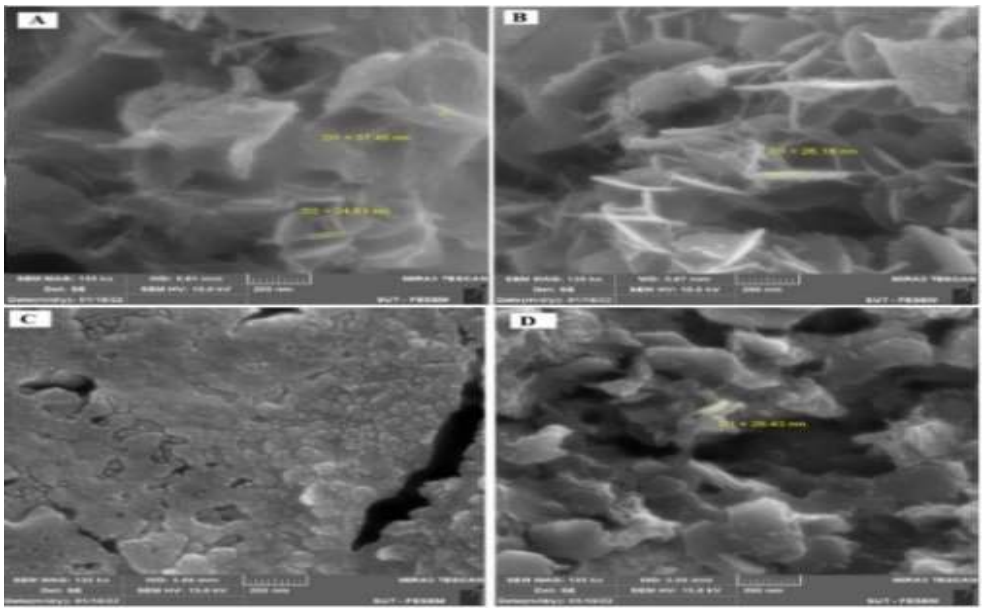

Figure 3: SEM images of AZO NPs prepared by 400 mJ at (A) 0.3 wt% Al ratio without magnetic field(B) 0.3 wt% Al ratio with the magnetic field (C) 0.5 wt% Al ratio without magnetic field and (D) 0.5 wt% Al ratio with the magnetic field (D).

Figure (4) shows the UV-Visible absorbance curves and the Tauc calculation of energy bandgap for the ZnO: $Al_{0.3\ wt\%}$ and ZnO: $Al_{0.5\ wt\%}$ prepared in distilled water in the absence and presence of a magnetic field. A strong absorption appeared at a low wavelength [24]. An Excitonic absorption peak was observed below the wavelength of the 358 nm bandgap (E_g = 3.46 eV). The sharp absorption peak of ZnO specifies the high crystallinity of the samples prepared with the magnetic field [25]. The absorption increased with the magnetic field as a result of increasing the ablation yield by enhancing the breakdown induced by the laser. The absorption edge blue-shifted (an increase of the optical bandgap) with the magnetic field due to a reduction in crystallite size, which causes the quantum confinement effect. On the other hand, increasing the Al content reduced the optical bandgap energy from 3.3 and 3.9 eV to 2.7 and 3 eV for the sample prepared without and with a magnetic field, respectively.

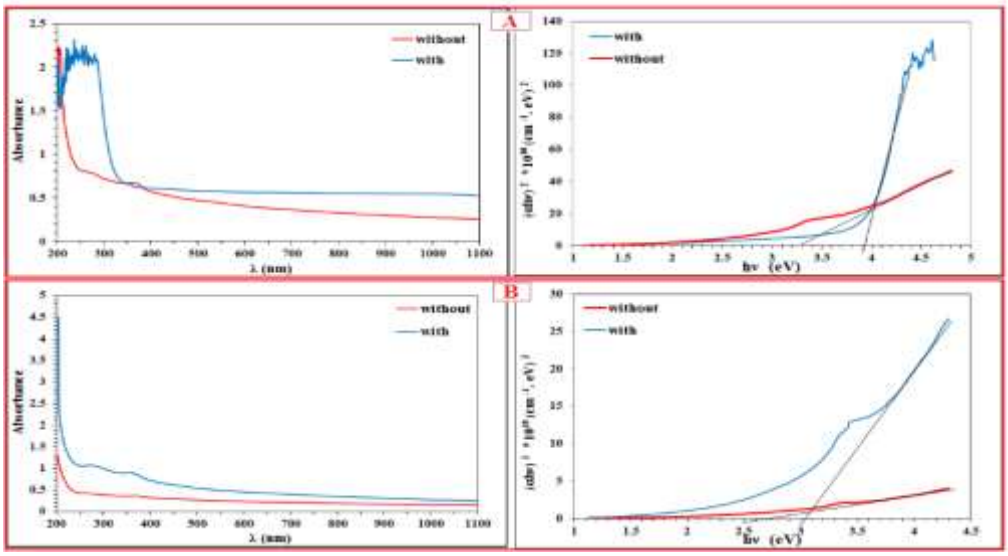

Figure 4: UV-Visible spectra and Tauc calculation for energy bandgap of AZO thin films prepared without and with the magnetic field using 400 mJ at (A)0.3 wt% Al ratio (B) and 0.5 wt% Al ratio.

The prepared AZO NPs were characterized using FTIR, as shown in Figure (5), for ZnO: $Al_{0.3\ wt\%}$ and ZnO: $Al_{0.5\ wt\%}$ prepared without and with the presence of the magnetic field. All spectra showed the characteristic band for the Zn-O band located around 490 cm^{-1} wavenumber [24]. The additional bands around 3300 cm^{-1} and 1650 cm^{-1} correspond to the stretching and bending vibration of O-H groups of water molecules absorbed from the ambient [26]. The Zn-O band increase in intensity with the presence of a magnetic field indicates the increase of the sample crystallinity. This band was reduced and small shifted to larger wavenumbers with increasing the laser energy and the Al ratio, indicating the variation in the bond length.

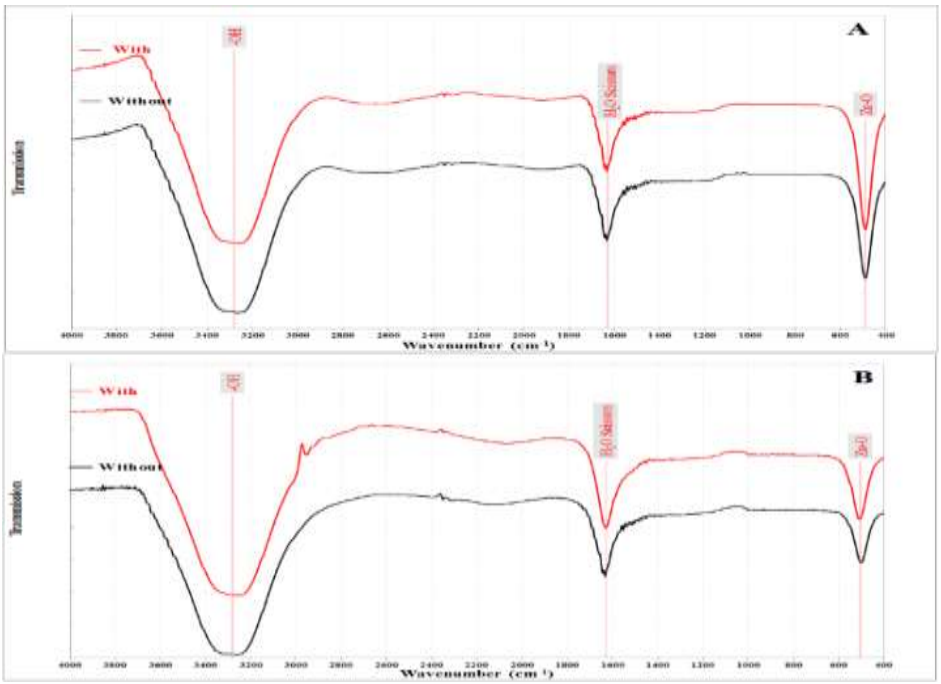

Figure 5: FTIR spectra of AZO thin films prepared without and with the magnetic field using 400 mJ at (A) 0.3 wt% Al ratio and (B) 0.5 wt% Al ratio.

The resistance variation of the prepared AZO thin film, with and without magnetic field, when exposed to 100 ppm NO_2 gas at different operating temperatures (150, 200, 250, and 300 °C) for the two Al ratios (0.3 wt% and 0.5 wt%) is shown in Figure (6) and (7), respectively. All samples behaved as n-type semiconductors by the increase in resistance with the oxidized gas exposure. Oxygen molecules are adsorbed on the active layer surfaces and extract electrons from the conduction band of the n-type semiconductor forming negative oxygen ions on the surface and a depletion layer in the sample. This action reduces the conductance due to reducing the charge carrier concentration or carrier mobility. With the NO_2 gas flowing, more electrons were extracted from the sample due to the interaction of the oxidizing gas with the oxygen species [27].

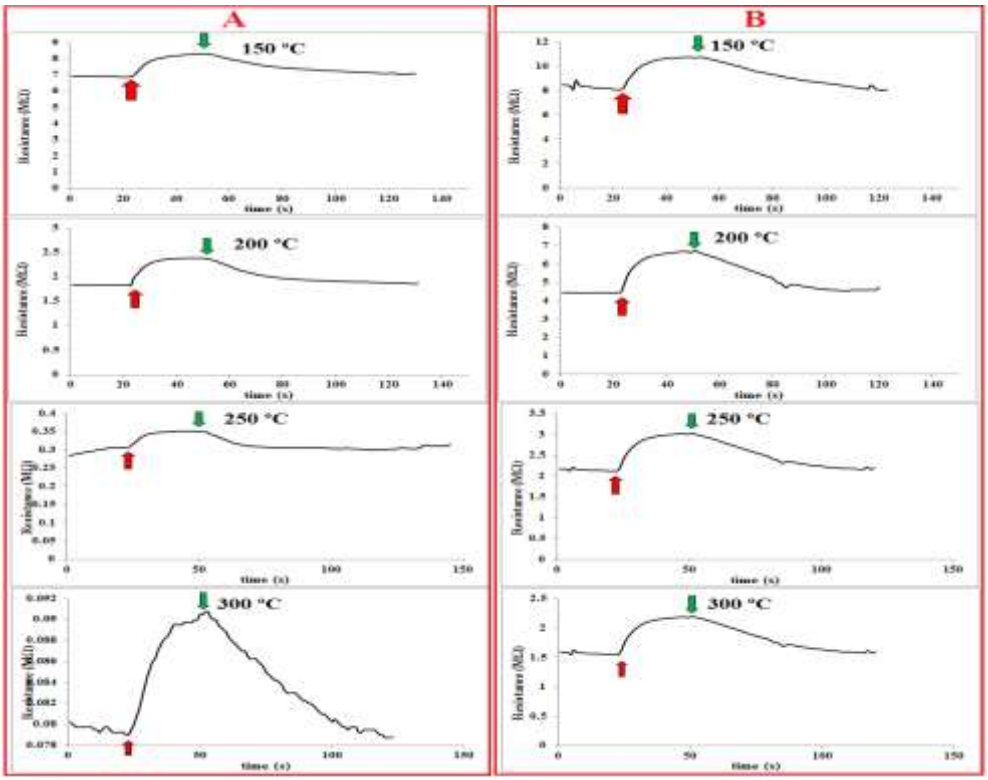

Figure 6: The resistance variation with time at different operation temperatures for ZnO: $Al_{0.3\ wt\%}$ (A) without and (B) with the magnetic field for 100 ppm NO_2 gas concentration.

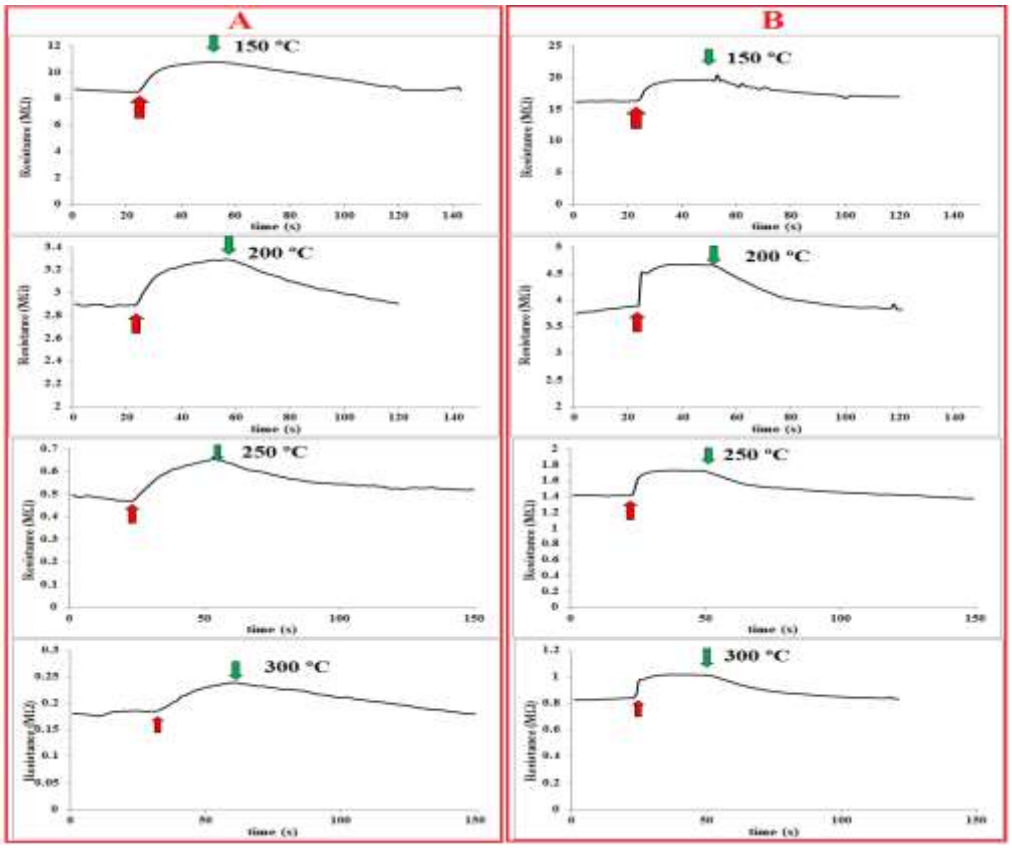

Figure 7: The resistance variation with time at different operation temperatures for ZnO: $Al_{0.5\ wt\%}$ (A) without and (B) with the magnetic field for 100 ppm NO_2 gas concentration.

The sensitivity of the AZO-based gas sensors using the different samples was determined according to the relation $S = (R_{gas}-R_{air}) / R_{air} \times 100\%$. The sensitivity of ZnO: $Al_{0.3\ wt\%}$ films increased with increasing the operating temperature to the optimum temperature of 200 °C with a sensitivity of 31.7% and 44.9% for samples prepared without and with the magnetic field, respectively. While the optimum operating temperature was 250 °C for ZnO: $Al_{0.5\ wt\%}$ films with a sensitivity of 36.8% and 21.4% without and with the magnetic field, respectively, as shown in Figure (8) and Table (2). The results indicated that the increased surface area with nano-plate structures of the ZnO: $Al_{0.3\ wt\%}$ sample enhances the sensitivity. The adsorbed O_2 from the ambient extracts electrons from the sample and forms different ion species depending on temperature. At low temperatures, the O_2^- is dominant; increasing the temperature, O^- is dominant and attracts more electrons from the sample. At higher temperatures, the adsorbed gases dissociate from the sample surface, causing a reduction in the sample response [28]. Response time and recovery time were evaluated from 90% of the resistance variation [29]. The added impurities may be associated with increased oxygen vacancies caused by the ZnO: Al lattice, which is the main factor in the gas sensing mechanism [30], [31].

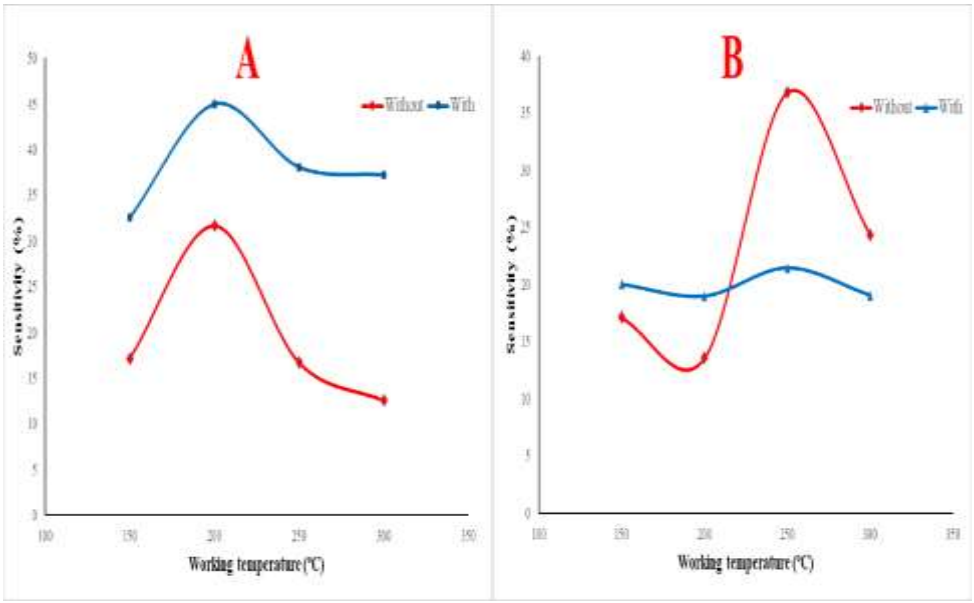

Figure 8: The variation of sensitivity of (A) ZnO: $Al_{0.3\ wt\%}$ and (B) ZnO: $Al_{0.5\ wt\%}$ with the operating temperature for 400mJ without and with the magnetic field for NO_2 gas.

Table 2: Gas sensor parameters (sensitivity, response time and recovery time) of the ZnO: $Al_{0.3\ wt\%}$ and ZnO: $Al_{0.5\ wt\%}$ without and with the magnetic field against NO_2 gas.

Al ratio	Temp (°C)	Without magnetic field			With magnetic field		
		Sensitivity%	Res. Time (s)	Rec. Time (s)	Sensitivity%	Res. Time (s)	Rec. Time (s)
0.3	150	17.1	20.0	50.0	32.5	20	50
	200	31.7	17.0	40.0	44.9	15	40
	250	16.7	10.0	20.0	38.0	15	40
	300	12.5	20.0	50.0	37.2	15	30
0.5	150	17.1	15.0	60.0	20.0	10	60
	200	13.5	20.0	50.0	19.0	8	45
	250	36.8	25.0	45.0	21.4	8	45
	300	24.3	25.0	65.0	19.0	8	30

Figures (9) and (10) illustrate the resistance variation of ZnO: $Al_{0.3\ wt\%}$ and ZnO: $Al_{0.5\ wt\%}$ samples prepared without and with the magnetic field, respectively, when exposed to 100 ppm concentration of H_2S. The AZO-based sensors were tested at different working temperatures (150, 200, 250, and 300 °C). The reducing gas reacts with the oxygen species absorbed from the ambient, resulting in the rapid uptake of the oxygen ions from the surface and liberating electrons to the semiconductor, causing a reduction in the resistance of the n-type by thinning the depletion region or increasing the carrier concentration. The sensor resistance returns to its initial value when exposed to ambient air [32].

As shown in Table (3), the sensitivity of the AZO-based gas sensor to H_2S gas increased with the increase of the operating temperature to reach the optimum values at optimum operating temperatures. The higher sensitivity corresponding to their optimal operating temperature of 250 °C increased with the presence of a magnetic field from 11.8% to 16.6% for the 0.3 wt% Al sample and from 16.7% to 26.7% for the 0.5 wt% Al sample, due to the different nanostructure construction with high surface area for the samples prepared with the presence of magnetic field [23].

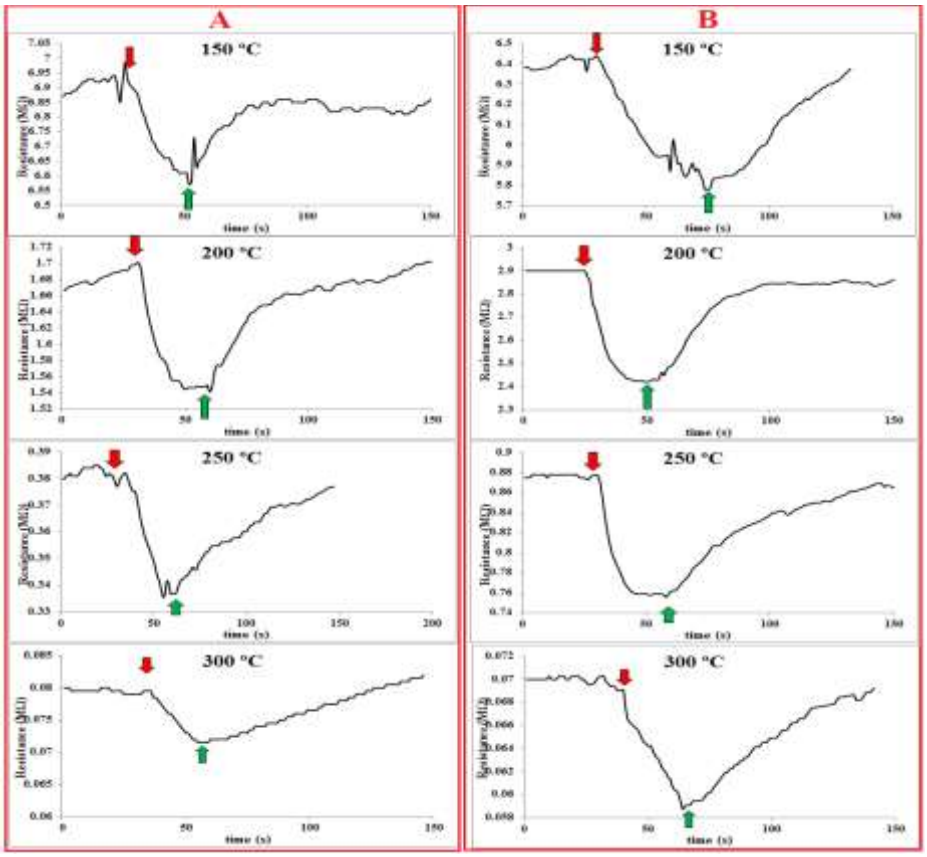

Figure 9: The resistance variation with time in different operation temperatures for ZnO: $Al_{0.3\ wt\%}$ (A)without and (B) with the magnetic field against H_2S gas.

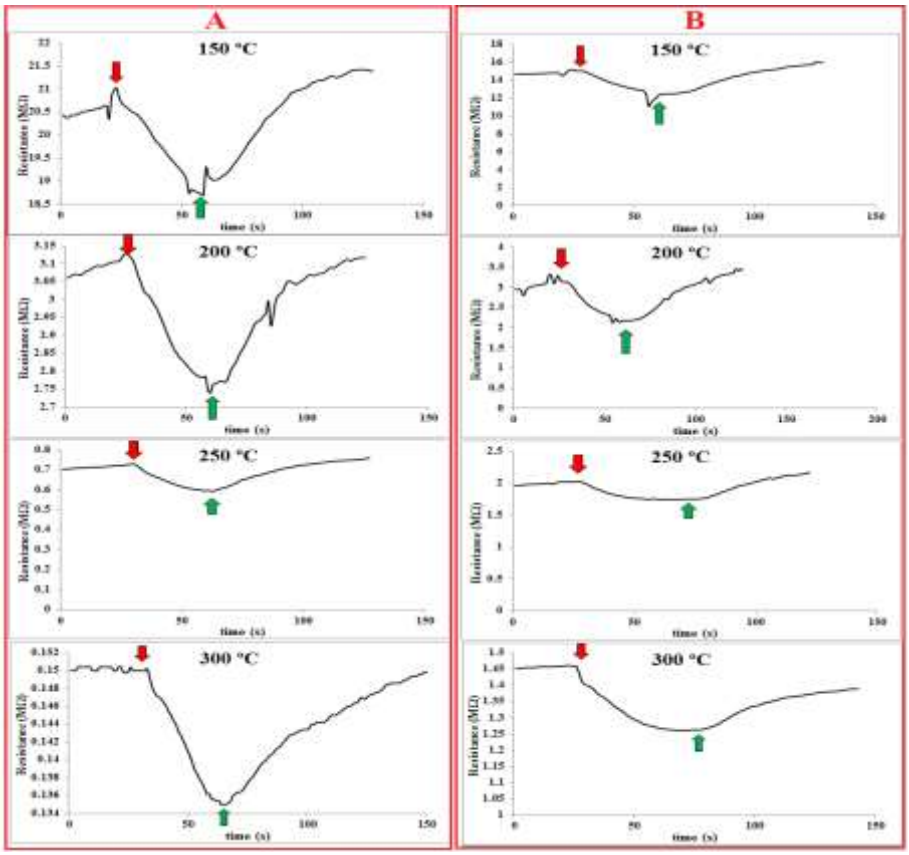

Figure 10: The resistance variation with time in different operation ttemperatures for ZnO: $Al_{0.5\ wt\%}$ (A) without and (B)with the magnetic field against H_2S gas.

The sensitivity of the gas sensor decreased at high operating temperatures due to the diffusion process of adsorbed gasses at high temperatures, as shown in Figure (11). The AZO samples had a higher response to the NO_2 gas than the H_2S gas due to the variation in the selectivity of the AZO sample of the two gasses.

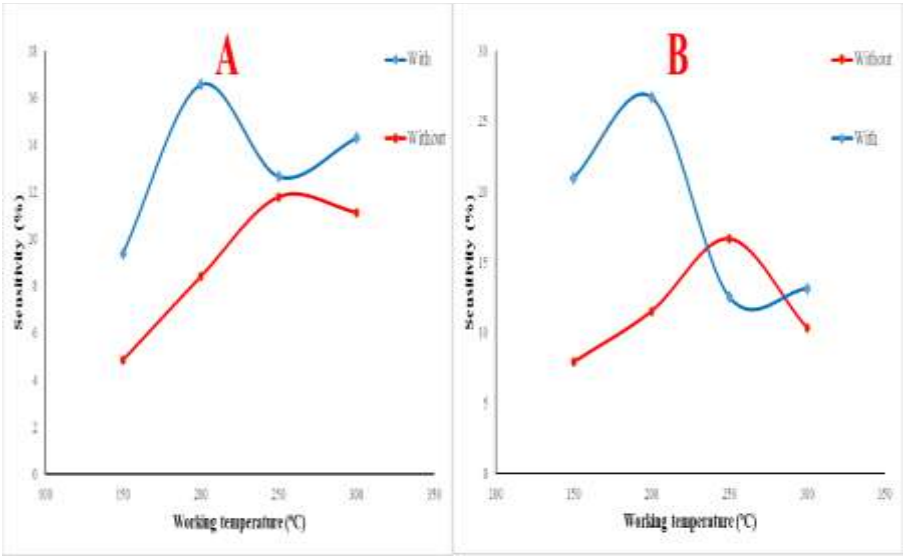

Figure 11: The variation of sensitivity with the operating temperature of the ZnO: $Al_{0.3\ wt\%}$ (A)and ZnO: $Al_{0.5\ wt\%}$ (B) for 400 mJ without and with the magnetic field for H_2S gas.

Table 3: Gas sensor parameters of the ZnO: $Al_{0.3\ wt\%}$ and ZnO: $Al_{0.5\ wt\%}$ without and with the magnetic field against H_2S gas.

Al ratio	Temp (°C)	Without Magnetic field			With Magnetic field		
		Sensitivity%	Res. Time (s)	Rec. Time (s)	Sensitivity%	Res. Time (s)	Rec. Time (s)
0.3	150	4.8	25.0	30.0	9.4	30	50
	200	8.4	20.0	40.0	16.6	25	40
	250	11.8	15.0	50.0	12.6	20	50
	300	11.1	20.0	70.0	14.3	20	40
0.5	150	7.9	25.0	50.0	20.9	20	55
	200	11.5	25.0	50.0	26.7	20	50
	250	16.7	30.0	60.0	12.5	25	30
	300	10.3	30.0	70.0	13.1	30	35

4. Conclusion

Zinc oxide: Aluminium composite nanostructures were prepared by the one-step PLAL method. The effect of applying an external magnetic field during the ablation process in distilled water creates distinctive nano-plates of thin thickness connected among each other; this structure is of a high surface area, which is an essential property to enhance gas sensing properties based on nanostructures. The XRD shows reduction in the crystallite size. Increasing the Al ratio from 0.3 wt% to 0.5 wt% in gas sensing applications causes a negative effect, it reduces the sample porosity. Hence, a limited percentage of added Al is a crucial parameter for the sensing performance. The construction of nanostructures with large surface for gas sensing purposes can be achieved using a permanent magnet placed behind the target during laser ablation in liquid or using a specific Al ratio. The prepared gas sensing detector response against NO_2 gas is higher than that of H_2S gas at an optimal operating temperature of 200 and 250°C depending on the existence of a magnetic field during ablation process.

References

[1] C. Tsay, K.-S. Fan, S.-H. Chen, and C.-H. Tsai, "Preparation and characterization of ZnO transparent semiconductor thin films by sol–gel method," *J. Alloys Compd.*, vol. 495, no. 1, pp. 126–130, 2010.

[2] C. Li, Y. Li, Y. Wu, B.-S. Ong, and R.-O. Loutfy, "Fabrication conditions for solution-processed high-mobility ZnO thin-film transistors," *J. Mater. Chem.*, vol. 19, no. 11, p. 1626, 2009.

[3] A. Wibowo, M. A. Marsudi, M. I. Amal, M. B. Ananda, R. Stephanie, H. Ardy, and L. J. Diguna, "ZnO nanostructured materials for emerging solar cell applications," *RSC Adv.*, vol. 10, no. 70, pp. 42838–42859, 2020.

[4] C. Li, X. Fan, L. Yu, L. Cui, M. Yin, Y. Li, N. Nan, and N. Liu, "A resistive-type UV detector based on ZnO nanowalls decoated by Ag nanowires," *Opt. Mater. (Amst).*, vol. 103, p. 109891, 2020.

[5] S. Nie, D. Dastan, J. Li, W.-D. Zhou, S.-S. Wu, Y.-W. Zhou, and X.-T. Yin, "Gas-sensing selectivity of n-ZnO/p-Co3O4 sensors for homogeneous reducing gas," *J. Phys. Chem. Solids*, vol. 150, p. 109864, 2021.

[6] A. F. Abdulrahman, S. M. Ahmed, N. M. Ahmed, and M. A. Almessiere, "Enhancement of ZnO Nanorods Properties Using Modified Chemical Bath Deposition Method: Effect of Precursor Concentration," *Crystals*, vol. 10, no. 5, p. 386, 2020.

[7] D. T. Speaks, "Effect of concentration, aging, and annealing on sol gel ZnO and Al-doped ZnO thin films," *Int. J. Mech. Mater. Eng.*, vol. 15, no. 1, p. 2, 2020.

[8] A. K. Abbas, K. A. Aadim, and E. J. Muhammed, "Spectroscopic studying of plasma parameters for PbS prepared by pulse Nd:YAG laser deposition," *AIP Conf. Proc.*, vol. 2372, no. 42, pp. 125–135, 2021.

[9] A. K. Jeryo and Q. A. Abbas, "Synthesis of Graphene Oxide Nanoparticles by Laser Ablation System," *Iraqi J. Sci.*, pp. 2241–2250, 2020.
[10] Z. M. Abbas and Q. Adnan, "Influence of Magnetic Field on Silver Nanoparticles Synthesized by Laser Ablation," *Iraqi J. Sci.*, pp. 341–350, 2020.
[11] Q. A. Abbas, "Effect of Target properties on the Plasma Characteristics that produced by Laser at Atmospheric Pressure," *Iraqi J. Sci.*, pp. 1251–1258, 2019.
[12] M. Schäfer, P. N. Terekhin, Y. Kang, G. Torosyan, X. del Arco Fargas, S. Hirtle, B. Rethfeld, and J. A. L'huillier, "Magnetic-field assisted laser ablation of silicon," *J. Opt. Soc. Am. B*, vol. 38, no. 12, p. E1, 2021.
[13] Z. A. Abbas and Q. A. Abbas, "Influence of the magnetic field on the characteristic of Au nanoparticles prepared by laser ablation," *AIP Conf. Proc.*, vol. 2372, no. 1, p. 080006, 2021.
[14] T. H. Kim, S. H. Nam, H. S. Park, J. K. Song, and S. M. Park, "Effects of transverse magnetic field on a laser-produced Zn plasma plume and ZnO films grown by pulsed laser deposition," *Appl. Surf. Sci.*, vol. 253, no. 19, pp. 8054–8058, 2007.
[15] M. Özgür, S. Pat, R. Mohammadigharehbagh, C. Musaoğlu, U. Demirkol, S. Elmas, S. Özen, and Ş. Korkmaz, "Al doped ZnO thin film deposition by thermionic vacuum arc," *J. Mater. Sci. Mater. Electron.*, vol. 30, no. 1, pp. 624–630, 2019.
[16] B. Liu and H. C. Zeng, "Hydrothermal Synthesis of ZnO Nanorods in the Diameter Regime of 50 nm," *J. Am. Chem. Soc.*, vol. 125, no. 15, pp. 4430–4431, 2003.
[17] S. Vempati, J. Mitra, and P. Dawson, "One-step synthesis of ZnO nanosheets: a blue-white fluorophore," *Nanoscale Res. Lett.*, vol. 7, no. 1, p. 470, 2012.
[18] N. Tripathy, R. Ahmad, H. Kuk, Y.-B. Hahn, and G. Khang, "Mesoporous ZnO nanoclusters as an ultra-active photocatalyst," *Ceram. Int.*, vol. 42, no. 8, pp. 9519–9526, 2016.
[19] W. S. Hussein, A. F. Ahmed, and K. A. Aadim, "Influence of Laser Energy and Annealing on Structural and Optical Properties of CdS Films Prepared by Laser Induced Plasma," *Iraqi J. Sci.*, pp. 1307–1312, 2020.
[20] M. M. ElFaham, M. Okil, and A. M. Mostafa, "Effects of post-laser irradiation on the optical and structure properties of Al 2 O 3 nanoparticles produced by laser ablation," *J. Appl. Phys.*, vol. 128, no. 15, p. 153104, 2020.
[21] A. F. Ahmed, F. A.-H. Mutlak, and Q. A. Abbas, "Evaluation of cold plasma effect to achieve fullerene and zinc oxide-fullerene hydrophobic thin films," *Appl. Phys. A*, vol. 128, no. 2, p. 147, 2022.
[22] A. G. Ardakani and P. Rafieipour, "Using ZnO nanosheets grown by electrodeposition in random lasers as scattering centers: the effects of sheet size and presence of mode competition," *J. Opt. Soc. Am. B*, vol. 35, no. 7, p. 1708, 2018.
[23] M. A. Kadhim, A. A. Ramadhan, M. O. S. Al-Gburi, G. J. Habi, and N. J. Hentawe, "Effect of Mixing Ratio of (SnO2)1-x(In2O3)x Thin Film on Gas Sensitivity," *Karbala Int. J. Mod. Sci.*, vol. 6, no. 1, pp. 83–92, 2020.
[24] P. K. Kannan, R. Saraswathi, and J. B. B. Rayappan, "CO2gas sensing properties of DC reactive magnetron sputtered ZnO thin film," *Ceram. Int.*, vol. 40, no. 8 part B, pp. 13115–13122, 2014.
[25] D. Patidar, A. Kaswan, N. S. Saxena, and K. Sharma, "Monodispersed ZnO Nanoparticles and Their Use in Heterojunction Solar Cell," *Sci. World J.*, vol. 2013, pp. 1–6, 2013.
[26] I. M. McIntosh, A. R. L. Nichols, K. Tani, and E. W. Llewellin, "Accounting for the species-dependence of the 3500 cm −1 H 2 O t infrared molar absorptivity coefficient: Implications for hydrated volcanic glasses," *Am. Mineral.*, vol. 102, no. 8, pp. 1677–1689, 2017.
[27] K. Schneider and W. Maziarz, "V2O5 Thin Films as Nitrogen Dioxide Sensors," *Proceedings*, vol. 2, no. 259, pp. 1–5, 2018.
[28] M. O. Salman, M. A. Kadhim, and A. A. Khalefa, "CdO : SnO 2 Composite UV-Assisted Room Temperature Ozone Sensor," *Iraqi J. Sci.*, vol. 64, no. 3, pp. 1190–1202, 2023.
[29] H. Xuemei, S. Yukun, and B. Bo, "Fabrication of Cubic p-n Heterojunction-Like NiO/In2O3 Composite Microparticles and Their Enhanced Gas Sensing Characteristics," *J. Nanomater.*, vol. 2016, pp. 1–9, 2016.
[30] R. S. Mohammed, K. A. Aadim, and K. A. Ahmed, "Spectroscopy Diagnostic of Laser Intensity Effect on Zn Plasma Parameters Generated by Nd: YAG Laser," *Iraqi J. Sci.*, vol. 63, no. 9, pp. 3711–3718, 2022.

[31] Y. F. Sun, S. B. Liu, F. L. Meng, J. Y. Liu, Z. Jin, L. T. Kong, and J. H. Liu, "Metal oxide nanostructures and their gas sensing properties: A review," *Sensors*, vol. 12, no. 3, pp. 2610–2631, 2012.

[32] D. Liu, Z. Tang, and Z. Zhang, "Comparative study on NO2 and H2S sensing mechanisms of gas sensors based on WS2 nanosheets," *Sensors Actuators B Chem.*, vol. 303, p. 127114, 2020.